

# COMPUTATION OF COLLISION PROBABILITIES BASED ON SPECIAL PERTURBATIONS AND HIGH ORDER METHODS

A. Morselli, R. Armellin, P. Di Lizia, and F. Bernelli Zazzera

*Politecnico di Milano, Department of Aerospace Sciences and Technologies, via La Masa 34, 20156 Milano, Italy  
Email: alessandro.morselli@mail.polimi.it, {roberto.armellin, pierluigi.dilizia, franco.bernelli}@polimi.it*

## ABSTRACT

A method for the identification of orbital conjunctions and the computation of the collision probability between two space objects is presented. The method is based on the Taylor expansion of both the time and the distance of closest approach between the two orbiting objects with respect to their uncertain initial positions and velocities. The collision probability is then computed via Monte Carlo simulations, taking advantage of the availability of analytical information to speed up the analysis. The efficiency of the proposed approach is further improved by adopting two advanced Monte Carlo techniques: Line Sampling and Subset Simulation. The resulting method applies on a wide range of orbits since no simplifications on the conjunction event are assumed. Test cases are run on LEO and GEO encounters. The standard and advanced Monte Carlo methods are compared in terms of collision probabilities and computational efficiency.

Key words: Orbital conjunctions; Differential algebra; Collision probability; Line Sampling; Subset Simulation.

## 1. INTRODUCTION

Collision probability plays an important role in the collision risk assessment between spacecraft and orbital debris. Its value is used to discriminate future conjunctions and determine how likely a collision between the two objects can occur. Different methods exist for the computation of this quantity. Most of these approaches [4, 1, 12] have the following assumptions in common:

- position uncertainties of the two objects are not correlated;
- both objects move along straight lines at constant velocities during the conjunction. This is true when its duration is limited to a few seconds;
- the uncertainties in the velocities can be neglected. This is valid since typical velocity errors are of the order of few m/s and the conjunction duration is limited;

- position uncertainty during the encounter is constant and equal to the value at estimated conjunction. This is a consequence of the previous assumption;
- the position uncertainties of the two objects are represented by three-dimensional Gaussian distributions.

According to these assumptions, the error covariance matrix of the positions of the two objects, mapped at the time of closest approach  $t^*$ , can be combined into a  $3 \times 3$  covariance matrix  $C$ . The collision probability is obtained by integrating the probability density function over the hard-body volume  $V_c$ . The volume integral reduces to a bidimensional integral on the B-plane.

Methods tailored for long-term encounters are present in literature [13, 7]. An approach that uses a set of consecutive linear segments to compute collision probability can be found in [2, 10].

Collision probability can be also computed by means of Monte Carlo (MC) simulations. The initial conditions of the two objects are sampled from their uncertainty distribution and propagated from  $t_0$  to the time of closest approach. For each couple of final positions, the relative distance  $d^*$  at the closest approach is computed and compared with the collision threshold  $D$ , which is defined as the diameter of the sphere enclosing the two objects. The collision probability is equal to the ratio between number of samples for which  $d^* < D$  and the total number of samples. The advantage of this approach lies in its generality, since assumptions of analytical methods can be dropped and it allows computations for complex object shapes.

Monte Carlo methods were also used to study the impact of non-Gaussian error volumes on collision probability computation [9]. Its drawback though is the high computational effort: each trajectory has to be propagated to the time of the close encounter. In recent times, to cope with this issue, techniques such as importance sampling [8] and adaptive splitting [11] have been applied to the problem of computing collision probability.

This paper aims at solving the above issues by merging the advantages of Monte Carlo methods and Differential

Algebra (DA). While retaining the main advantages of Monte Carlo simulations (i.e. no limiting assumption are made on object dynamics and encounter geometry), the proposed approach gains efficiency in terms of computational effort. The method is thus suitable for both long-term and short-term encounters, addressing the effect of velocity uncertainties. Consequently, it can be applied to the challenging problem of geosynchronous orbits, where relative velocity between the spacecraft is low.

First, the objects dynamics are numerically propagated taking into account the main sources of perturbations (geopotential acceleration, atmospheric drag, solar radiation pressure, and third body). Since this propagation is performed in the DA framework, an arbitrary order Taylor expansion of the flow is obtained. The stationarity of the square distance during the close approach is then imposed and partial inversion techniques are used to obtain the Taylor expansion of  $d^*$  and  $t^*$  with respect to the initial uncertainties. The polynomial approximation of  $d^*$  allows to rapidly estimate the distance of closest approach for each couple of virtual objects by means of fast polynomial evaluations.

The paper is organized as follows: in Sect. 2 some hints on how a numerical integration of the dynamics is performed in the DA framework are given. The procedure for the computation of the Taylor expansion of the time and distance of closest approach is described in Sect. 4. The Monte Carlo methods are described in Sect. 5, and details on the advanced methods of Line Sampling (LS) and Subset Simulation (SS) are given in Sect. 5.1 and 5.2 respectively. Numerical results and experiments are provided in Sect. 6.

## 2. DIFFERENTIAL ALGEBRAIC TECHNIQUES

The dynamical model and the integrations performed within this paper take advantage of the tool COSY-Infinity [5], which implements differential algebra. Differential algebraic techniques allow the derivatives of any function to be computed up to an arbitrary order with limited effort in a computer environment [6].

Differential algebra finds its main application in the fast computation of high order Taylor expansions of the flow of ordinary differential equations (ODEs). In particular, any integration scheme is based on algebraic operations, involving the evaluation of the ODE right hand side at several integration points. If all operations are carried out in the DA framework, then it is possible to obtain the arbitrary order expansion of the flow of a general ODE with respect to the initial conditions [14]. Without loss of generality, consider the scalar initial value problem

$$\begin{cases} \dot{x} = f(x, t) \\ x(t_0) = x_0 \end{cases} \quad (1)$$

with its associated phase flow  $\varphi(t; x_0)$  and the forward

Euler's schemes

$$x_i = x_{i-1} + f(x_{i-1}) \Delta t. \quad (2)$$

If the initial condition  $x_0$  is initialized as a DA variable, considering the constant part and the first derivative, i.e

$$[x_0] = x_0 + \delta x_0, \quad (3)$$

then, at the first time step we have

$$[x_1] = [x_0] + f([x_0]) \cdot \Delta t. \quad (4)$$

The output of the first step is the  $k$ -th order Taylor expansion of the flow  $\varphi(t; x_0)$  in  $x_0$  for  $t = t_1$ . The result of the final step is the  $k$ -th order Taylor expansion of  $\varphi(t; x_0)$  in  $x_0$  for  $t = t_f$ , where several non-zero coefficients corresponding to high order terms in  $\delta x_0$  appears. In addition, when the final time is initialized as a DA variable

$$[t_f] = t_f + \delta t_f, \quad (5)$$

the high order expansion of the flow with respect to final time is gained too. This consideration is crucial for the procedure illustrated in Sec. 4.

An advantage of the DA-based approach is that there is no need to write and integrate variational equations to obtain the high order expansion of the flow but it is sufficient to replace the operations between real numbers with adjoint operations on DA numbers.

## 3. DYNAMICAL MODEL

The numerical propagator AIDA (Accurate Integrator for Debris Analysis) have been developed by the authors and is used to compute the objects position and velocity at a given time instant. AIDA is based on Differential Algebra and is written in COSY-Infinity. The perturbations modeled in AIDA are

1. atmospheric drag, using density model NRLMSISE-00 that includes anomalous oxygen,
2. geopotential acceleration, using EGM2008 model,
3. solar radiation pressure with dual-cone shadow,
4. Sun and Moon gravitational attraction.

The following assumptions are made for the analyses carried out within this paper: the degree and order of the gravitational spherical harmonics is set to 10; the atmospheric drag is supposed to affect object dynamics for altitudes below 2000 km; Sun and Moon position, required by third body and solar radiation pressure computations, are obtained from NASA DE405 ephemeris.

The numerical integrator used in AIDA is a DA version of the Dormand and Prince (8-th order solution for propagation, 7-th order solution for step size control) implementation of Runge-Kutta integrator.

#### 4. EXPANSION OF TIME AND DISTANCE OF CLOSEST APPROACH

The aim of this procedure is to obtain the Taylor expansion of time  $t^*$  and distance  $d^*$  of closest approach with respect to the uncertainties in the initial conditions of the two objects

$$\begin{aligned} [t^*] &= t^* + (\delta \mathbf{x}_0^1, \delta \mathbf{x}_0^2) \\ [d^*] &= d^* + (\delta \mathbf{x}_0^1, \delta \mathbf{x}_0^2), \end{aligned} \quad (6)$$

where  $\mathbf{x}_0^1$  and  $\mathbf{x}_0^2$  are six elements vector, i.e. gathering initial position and velocity of each object in ECI reference frame (any set of orbital elements in any arbitrary reference frame can be used). Their uncertainties estimated from available Two-Line Elements sets or computed from orbit determination processes.

The procedure for the time and distance of closest approach identification and expansion is divided in the following steps:

1. compute first guesses of  $t^*$  and  $d^*$ . For example, this can be achieved with the technique described in [3], where all stationary points of the relative distance are obtained through rigorous global optimization, using SGP4/SDP4 propagator;
2. use AIDA to propagate the uncertain initial conditions from  $t_0$  to the first guess of  $t^*$ . The result is the Taylor expansion of final positions and velocities with respect to initial conditions and final time:

$$\begin{aligned} [\mathbf{r}_f^1] &= \mathbf{r}_f^1 + \mathcal{M}_{\mathbf{r}_f^1} (\delta t^*, \delta \mathbf{x}_0^1) \\ [\mathbf{r}_f^2] &= \mathbf{r}_f^2 + \mathcal{M}_{\mathbf{r}_f^2} (\delta t^*, \delta \mathbf{x}_0^2); \end{aligned} \quad (7)$$

3. compute the partial time derivative of the squared relative distance

$$[d^2] = ([\mathbf{r}_f^1] - [\mathbf{r}_f^2]) \cdot ([\mathbf{r}_f^1] - [\mathbf{r}_f^2]) \quad (8)$$

$$\left[ \frac{\partial d^2}{\partial t} \right] = c_0 + \mathcal{M}_{\frac{\partial d^2}{\partial t}} (\delta t^*, \delta \mathbf{x}_0^1, \delta \mathbf{x}_0^2) \quad (9)$$

and use partial inversion techniques to obtain  $\delta t^*$  as function of this derivative;

4. impose the derivative to be zero to compute the map that describes the change in  $t^*$  due to variations in  $\mathbf{x}_0^1$  and  $\mathbf{x}_0^2$

$$[t^*] = t^* + \mathcal{M}_{t^*} (\delta \mathbf{x}_0^1, \delta \mathbf{x}_0^2); \quad (10)$$

5. plug map (10) into final position maps of Eq. (7) to obtain the map of the distance of closest approach as function of both  $\mathbf{x}_0^1$  and  $\mathbf{x}_0^2$ .

Given any set of initial conditions sampled from their uncertain distribution, the associated  $t^*$  and  $d^*$  are obtained

by means of the fast evaluations of the resulting polynomials, drastically reducing the computational effort. In fact, the stationarity conditions of the closest approach are imposed right after partial inversion and the resulting map for  $t^*$  is directly plugged into the Taylor expansion of  $d^*$ . Thus, the values of  $d^*$  obtained by evaluating the resulting polynomials are the minima of the relative distance for each couple of virtual objects.

#### 5. COLLISION PROBABILITY COMPUTATION

Fast polynomial Monte Carlo methods for collision probability computation can be developed based on the available Taylor expansion of  $d^*$  and  $t^*$ . More specifically, the sets of initial conditions are sampled from their uncertainty distribution. Then, the values of  $d^*$  for each couple of virtual objects are computed evaluating the available polynomials. The number of samples  $N_c$  for which the collision condition, i.e.  $d^* < D$ , is verified are divided by the total number of samples  $N_T$  to compute the collision probability

$$P(d^* < D) = \frac{N_c}{N_T} \quad (11)$$

Using this approach no assumptions on the close approach are made, so the method is suitable for both long-term and short-term encounters. In addition, it drastically reduces the computational time with respect to standard Monte Carlo methods, where, for each couple of initial conditions, numerical propagations have to be performed. Nevertheless, similarly to standard Monte Carlo methods, the number of samples required to compute typical values of collision probability (i.e. of the order of  $10^{-4}$  or lower) with a decent accuracy is of the order of  $10^6$ . Thus, advanced Monte Carlo methods are used in this work to increase the efficiency and accuracy of collision probability computation. More specifically Subset Simulation (SS) and Line Sampling (LS) have been tested.

##### 5.1. Subset Simulation

Subset Simulation is an adaptive stochastic simulation method that can compute small probabilities as product of larger conditional probabilities

$$P(d^* < D) = P(F) = P(F_m) \prod_{i=1}^{m-1} P(F_{i+1}|F_i), \quad (12)$$

where  $m$  is the number of conditional levels and  $F_{i+1}$  indicates the region conditional to  $F_i$  [15]. The method is initialized with a standard Monte Carlo simulation with few samples. The samples are sorted according to their associated value of  $d^*$ . The ones for which the relative distance  $d^*$  is lower are used to generate other samples using Monte Carlo Markov Chains. These new samples all belong to conditional level  $F_1$  which is conditional to the initial volume  $F_0$ . This new set of samples is sorted

again and the samples with the lower  $d^*$  are identified and then used as seeds to generate new Markov Chains. This iterative process terminates when the threshold that identifies the new conditional level is below a collision threshold  $D$ .

## 5.2. Line Sampling

The main idea behind Line Sampling is transforming an high-dimensional problem into many 1D problems along an “important direction”  $\alpha$  [16]. This important direction is defined as

$$\alpha = -\frac{\nabla_{d^*}(\mathbf{x}_0^1, \mathbf{x}_0^2)}{\|\nabla_{d^*}(\mathbf{x}_0^1, \mathbf{x}_0^2)\|_2}, \quad (13)$$

where the elements of the gradient of  $d^*$  can be obtained as the first order coefficients of the expansion of  $d^*$ . Each sample is used to define the equation of a straight line passing through it and parallel to  $\alpha$ . The high-dimensional space is explored moving along this straight line, i.e. using only one parameter  $c$ . If the line intersects the failure region ( $d^* < D$ ), two boundary value  $c_1^k$  and  $c_2^k$  are identified for the sample  $k$ . The 1D probability becomes

$$\hat{P}^{1D,k}(d^* < D) = \Phi(c_1^k) - \Phi(c_2^k), \quad (14)$$

where  $\Phi(\cdot)$  is the standard normal cumulative distribution function. If the straight line does not intersect the failure region, the associated one-dimensional probability is zero. The collision probability is then computed as the mean value of all one-dimensional probabilities. The variance of  $P(d^* < D)$  can be computed as well.

## 6. NUMERICAL RESULTS

The algorithms for the calculation of collision probability described above have been tested with the three conjunctions listed in Table 1. The cases are sorted in decreasing relative velocity, and long-term and short-term encounters are considered.

Table 1. Test cases

Case	NORAD CAT ID	Orbit	$t^*$	$d^*$ [km]	$\Delta v$ [km/s]
A	20735	LEO	2013/2/21 21:51:38	0.186	8.854
	08544	LEO			
B	11750	LEO	2013/2/23 20:10:06	0.265	4.841
	23604	LEO			
C	18575	GEO	2013/2/26 21:54:13	3.417	0.774
	37238	GEO			

The collision probabilities obtained for test cases A, B, and C are listed in Table 2, together with the total number of samples  $N_T$  used for the computation, the computational time  $t_c$ , and the coefficient of variation (c.o.v.)

$\delta$ . Both uncertain initial positions and velocities are considered, assuming they are Gaussian. All simulations are performed on an Intel Core i5 2500 3.30 GHz, 8 Gb RAM processor running Sabayon Linux 10. The Taylor expansion of the dynamical flow is computed up to order 3.

Table 2. Collision probability with collision threshold  $D = 100 m$

Case		$P(F)$	$N_T$	$t_c$ [s]	$\delta$ -
A	MC	3.80E-5	1E6	114.61	0.162
	LS	3.89E-5	5000	11.64	0.031
	SS	3.77E-5	11600	11.98	0.315
B	MC	8.00E-6	1E6	120.43	0.354
	LS	1.36E-5	5000	10.16	0.037
	SS	1.15E-5	13200	13.21	0.411
C	MC	2.00E-6	1E6	128.33	0.707
	LS	1.36E-6	5000	8.48	0.184
	SS	1.37E-6	16400	16.61	0.822

The same number of samples is used for MC and LS, while the number of samples of SS changes due to its iterative procedure. The collision probabilities seem in good accordance in all test cases, although the accuracy of standard Monte Carlo simulation tends to decrease for collision probabilities below  $10^{-5}$ , as can be seen from test cases B and C. This is due to the fact that, for lower probabilities, fewer samples are found with  $d^*$  lower than the threshold  $D$ . In addition, the computational time of MC is almost 10 times larger than the ones of LS and SS, which range from 8 to 16 s.

To compare the efficiency of the three methods, two figures of merit can be introduced. The first figure of merit is the unitary coefficient of variation,  $\Delta$ , defined as

$$\Delta = \delta \sqrt{N_T} = \frac{\sigma(\hat{P}(F))}{\hat{P}(F)} \sqrt{N_T}. \quad (15)$$

The unitary c.o.v. is dimensionless and independent on  $N_T$ , since  $\delta \propto 1/\sqrt{N_T}$ . The lower is the value of  $\Delta$  the higher is the efficiency of the method. In Fig. 1 the  $\Delta$  computed for the three test case are compared. Note that in all test cases  $\Delta$  is normalized by the value computed for the corresponding Monte Carlo simulation.

According to these results, Line Sampling is the more efficient method, since its  $\Delta$  is two order of magnitude lower than the one of MC and one order of magnitude lower than the one of Subset Simulation.

The second figure of merit,  $\eta$ , takes into account the collision probability variance  $\sigma^2$  and the computational time  $t_c$

$$\eta = \frac{1}{\sigma^2(\hat{P}(F)) t_c}. \quad (16)$$

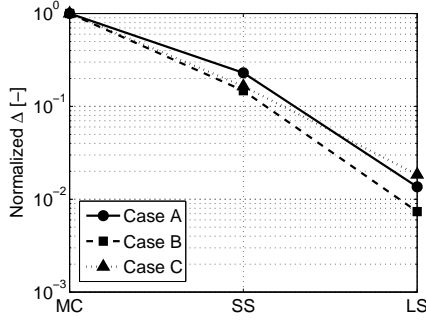


Figure 1. Normalized values of unitary c.o.v.  $\Delta$

Note that  $\eta$  does not depend on the number of samples  $N_T$  since  $t_c \propto N_T$  and  $\sigma^2 \propto 1/N_T$ . The higher is the value of  $\eta$  the higher is the efficiency of the method in terms of accuracy of the result and computational time. The values of  $\eta$  for each test case are plotted in Fig. 2. Similarly to Fig. 1  $\eta$  is normalized by the value obtained for the Monte Carlo simulation.

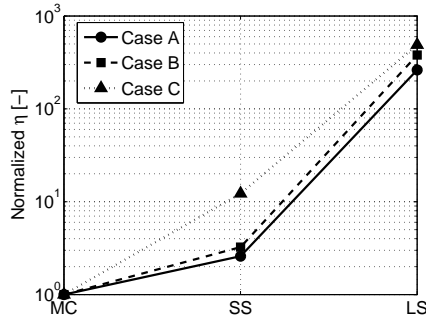


Figure 2. Normalized values of figure of merit  $\eta$

Once again, Line Sampling outperforms the other methods: the corresponding  $\eta$  are two order of magnitude higher than the one of Monte Carlo and Subset Simulation. It is worth observing that the efficiency of SS for test case C is higher than for cases A and B. This exalts the reliability of SS for the accurate computation of very low probabilities. Unlike LS, whose performances mainly depend on the number of samples used and the value of collision probability itself, the efficiency of SS depends on many parameters, such as the number of seed to be used to generate Markov Chains, the number of samples of each conditional level, and the parameters for Markov Chains generation. Thus, the efficiency of SS can be likely increased by suitably tuning the associated parameters.

## 6.1. Effect of velocity uncertainty

An analysis of the collision probability for varying covariance matrices is performed to study the effect of velocity uncertainty on the computed collision probability. Computations are performed by Taylor expanding  $t^*$  and  $d^*$  with respect to both uncertain initial positions and velocity, grouped in the state vector  $\delta x_0^1$  and  $\delta x_0^2$ , and with respect to uncertain initial positions  $\delta r_0^1$  and  $\delta r_0^2$  only. The results are compared by scaling the original covariance matrix by the same factor  $l \in [0.01; 5]$  and using LS to compute impact probability. The results are plotted in Fig. 3 for the test case with higher relative velocity (case A) and lower relative velocity (case C), with a collision threshold  $D = 100$  m. It is worth observing that the collision probabilities listed in Tab. 2 correspond to the point  $l = 1$  on the solid curves.

All curves have similar behavior: no collision is found for very small values of  $l$  since the value of the relative distance at the closest approach is larger than the threshold  $D$ . Collision probability then increases for larger  $l$  to a maximum value before starting decreasing. Note that the collision probabilities in the decreasing part of the curve are underestimated and need the knowledge on initial conditions to be refined to reduce uncertainty.

The dashed curves, corresponding to uncertain positions only, tend to shift up and right with respect to solid curves, obtained with uncertain positions and velocities. The effect is larger for case C, which is a long-term encounter in GEO. In this case the uncertainty on initial velocities plays a crucial role, since: in case it is not considered and  $l < 2$ , the resulting collision probability would be underestimated

The relative distance vectors  $\Delta r$  can be sampled and projected on the so called NT plane to approximate graphically their distributions. By definition the  $T$  versor is parallel to satellite velocity and  $N$  is perpendicular to the velocity and belongs to the orbital plane. In Fig. 4 the projections of  $\Delta r$  are plotted on the nominal NT plane corresponding to the first object of each pair, i.e. 20735 for test case A and 18575 for test case C. The grey dots are obtained considering only initial position uncertainty, whereas black dots are computed for uncertain positions and velocities. Note that the two axis are not on a 1:1 scale to emphasize differences in the distributions. For test case A no significant variation in the distribution of grey and black dots is found, and grey dots cover the area described by the black dots. The pattern is different for test case C, where the area described by the grey dots is smaller and seems slightly rotated. In addition grey region does not embrace the origin of the reference frame.

This helps explaining the results found in Fig. 3. Adding initial velocities as uncertain parameter seems not to affect the relative position distribution for test case A, which can be classified as a short-term encounter. Instead, uncertainties on  $v_0^1$  and  $v_0^2$  affect the distribution of  $\Delta r$  for test case C, which has a low nominal relative velocity during the close approach. The smaller extent

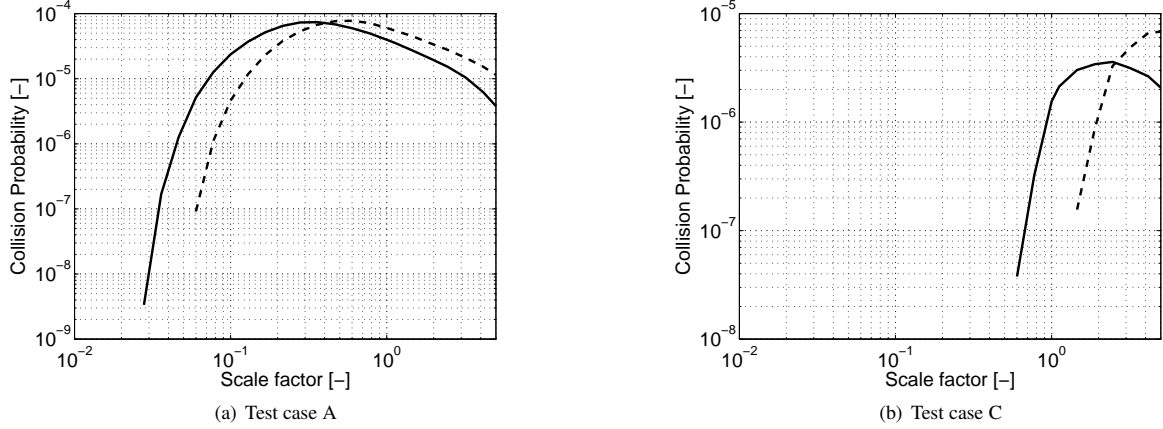


Figure 3. Collision probability vs. covariance scale factor  $l$ . Solid curves are obtained by setting uncertainties on both initial position and velocity, while dashed curves are for uncertain positions only.

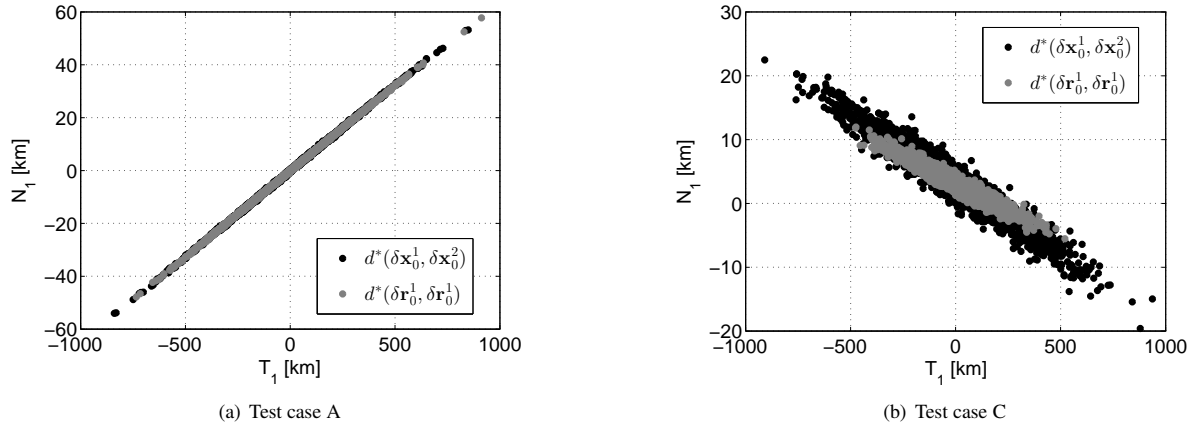


Figure 4. Relative distance vector projected on the NT plane of the first object for test cases A and C. Grey dots represents relative distance projections computed using uncertain initial positions only, black dots take into account both uncertain initial positions and velocities.

of the grey region, coupled with a nominal distance of closest approach of more than 3 km, turn out to decrease collision probability to zero: no relative position vectors are indeed sampled in the sphere of diameter  $D$ , centered in the origin of the reference frame. This confirms the result in Fig. 3(b), where a non-zero collision probability is found only for uncertain positions and velocities for  $l = 0$ .

## 7. CONCLUSIONS

A method for the computation of collision probability has been developed by merging DA expansion of time and distance of closest approach and Monte Carlo simulation. This approach enables a significant reduction of the computational effort, since the numerical propagation

of the orbital dynamics is substituted by polynomial evaluations, without loss of accuracy. The propagations accounts for the main sources of perturbation, using up-to-date models for spherical harmonics and air density. The procedure described for the expansion of  $d^*$  and  $t^*$  can be adapted to any set of initial states and using any arbitrary reference frame, which widens the applicability of the method to data coming from any special perturbation catalog.

Besides standard Monte Carlo simulations, two advanced Monte Carlo methods are used for the computation of collision probability, Line Sampling and Subset Simulation. Both methods have better performances in terms of computational time and accuracy with respect to Monte Carlo simulation, although the better results in terms of efficiency are obtained for Line Sampling. With only 5000 samples, LS can compute probabilities as low as  $10^{-8}$ .

Tests performed on both long-term and short-term encounters showed that the collision probabilities computed with the three methods are in good accordance. Being based on the Taylor expansion of  $d^*$  and  $t^*$  and since no assumptions are made on the dynamics of the encounter, the presented methods are also suitable for close encounters with low relative velocity. The capability of capturing the effect of velocity uncertainty has been studied. For GEO conjunctions it has been shown that the effect of uncertain velocity can lead to underestimation of collision probability.

Future studies will focus on the improvement of computational performance of the method. In particular all three methods can be parallelized with small effort. The codes can be classified as embarrassingly parallel, since the evaluation performed for each sample are independent one from the other. A comparison with the probability computed using analytical methods will be performed to investigate the validity of their assumptions and determine the limit of their applicability.

## ACKNOWLEDGMENTS

The authors are grateful to Martin Berz and Kyoko Makino for having introduced us to differential algebra techniques as well as for the implementation of COSY-Infinity, without which this work would not have been possible.

## REFERENCES

1. Akella M. R., Alfriend K. T., (2000). Probability of collision between space objects, *Journal of Guidance, Control, and Dynamics*, **23**(5), 769–772
2. Alfano S., (2006). Addressing nonlinear relative motion for spacecraft collision probability, *AIAA/AAS Astrodynamics Specialist Conference and Exhibit*, Keystone, CO
3. Armellin R., Morselli A., Di Lizia P., Lavagna M., (2012). Rigorous Computation of orbital conjunctions, *Advances in Space Research*, **50**(5), 527–538
4. Bèrend N., (1999). Estimation of the probability of collision between two catalogued orbiting objects, *Advances in Space Research*, **23**(1), 234–247
5. Berz M., Makino K., (2006). *COSY Infinity Version 9 Reference Manual*, Michigan State University Report
6. Berz M., (1999). *Differential Algebraic Techniques*, Entry in Handbook of Accelerator Physics and Engineering, World Scientific, New York
7. Chan K., (2004). Short-term vs Long-term spacecraft encounters, *AIAA/AAS Astrodynamics Specialist Conference and Exhibit*, Providence, RI.
8. Dolado J. C., Legendre P., Garmier R., Reveling B., Pena X., (2011). Satellite collision probability for long term encounters, *Advances in the Astronautical Sciences*, **142**
9. Ghrist R. W., Plakalovic D., (2012). Impact of non-Gaussian error volumes on conjunction assessment risk analysis. *AIAA/AAS Astrodynamics specialist conference*, Paper AIAA-2012-4965
10. McKinley D., (2006). Development of a nonlinear probability collision tool for the Earth observing system, *AIAA Journal*, Paper AIAA-2006-6295
11. Estimating satellite versus debris collision probability via the adaptive splitting technique, *3rd International Conference on Computer modeling and simulation*, Mumbai, India
12. Patera R. P., (2001). General method for calculating satellite collision probability, *Journal of Guidance, Control, and Dynamics*, **24**(4), 716–722
13. Patera R. P., (2003). Satellite collision probability for nonlinear relative motion, *Journal of Guidance, Control, and Dynamics*, **26**(5), 728–733
14. Valli M., Armellin R., Di Lizia P., Lavagna M., (2013). Nonlinear mapping of uncertainties in Celestial Mechanics, *Journal of Guidance, Control, and Dynamics*, **36**(1), 48–63
15. Zio E., Pedroni N., (2009). Estimation of the functional failure probability of a thermal-hydraulic passive system by Subset Simulation, *Nuclear Engineering and Design*, **229**(3), 580–599
16. Zio E., Pedroni N., (2009). Functional failure analysis of a thermal-hydraulic passive system by means of Line Sampling, *Reliability Engineering & System Safety*, **94**(11), 1764–1781